Supporting Information

Ion-Etching-Induced Defect Engineering toward Porous Fe–N–C for Efficient Oxygen Reduction Reaction

Yong Yang,[a] Kun-Zu Yang,[a] Ling Jia,[a] Hao-Ning Zhu,[a] Wen-Quan Yuan,[a] Ping-Jie Wei,[a] Chao Xu,[b] and Jin-Gang Liu *[a]*

[a]Key Lab for Advanced Materials, School of Chemistry & Molecular Engineering, East China University of Science and Technology, Shanghai, 200237, P. R. China. E-mail: liujingang@ecust.edu.cn
[b]State Key Laboratory of Chemical Engineering, East China University of Science and Technology, Shanghai, 200237, P. R. China. E-mail: chaoxu@ecust.edu.cn

1. Chemicals

All chemicals and solvents were obtained from commercial sources and used as-received without further purification. High-purity water (⩾18.25 MΩ·cm) and methanol were used to prepare the solutions.

2. Material synthesis

(1) Synthesis of ZIF-L

ZIF-L was obtained according to the reported literature. [1] Specifically, 0.595g of $Zn(NO_3)_2{\cdot}6H_2O$ and 1.3136g of 2-MeIm were separately dissolved in 40 mL of deionized water. The aqueous zinc nitrate solution was then added to the aqueous 2-MeIm solution under stirring. The mixture was stirred at room temperature for 4 hours. The resulting product was collected by centrifugation, washed with deionized water, and dried in an oven at 70°C.

(2) Synthesis of ZIF-R and pNC

ZIF-R was prepared by mixing $Zn(NO_3)_2{\cdot}6H_2O$ (0.100 g) and the pre-synthesized ZIF-L precursor (0.200 g) in co-solvent of DMF/ethanol (32 mL, V:V = 3 : 1). The mixture was treated by ultrasonication for 5 minutes and then heated at 70°C for 2 h. The resulting product was separated by centrifugation, washed several times with ethanol, and dried under vacuum. The dried ZIF-R was pyrolyzed under N_2 at 900°C for 1 h with a heating rate of 5°C min^{-1} to obtain pNC.

(3) Synthesis of d-Fe-N-C-x/T and d-Fe-N-C

20 mg of pNC were dispersed in 40 mL of methanol, followed by the addition of Fe $(NO_3)_3$ $9H_2O$. The mixture was stirred at 50 °C for 24 h. The resulting solid, denoted as d-Fe-N-C-x, was collected by centrifugation. After drying, the product was pyrolyzed at 800°C for 30 min with a heating rate of 5°C min^{-1} to obtain the final catalyst d-Fe-N-C. Here, x represents the mass of $Fe(NO_3)_3$ $9H_2O$ used (1, 2, 3, or 4 mg), and T indicates the pyrolysis temperature (700, 800, or 900°C).

(4) Synthesis of d_x-Fe-N-C

The added $Zn(NO_3)_2{\cdot}6H_2O$ amount was first adjusted to 50 mg and 200 mg, followed by pyrolysis to obtain pNC. The subsequent procedures were the same as those for d-Fe-N-C. The resulting catalysts with Zn salt additions of 50 mg and 200 mg were designated as $d_{0.5}$-Fe-N-C and d_2-Fe-N-C, respectively.

(5) Synthesis of Fe-N-C

The preparation process of Fe-N-C was the same as that of d-Fe-N-C, except that ZIF-L was not subjected to the Zn^{2+} etching step.

3. Material characterization

The morphologies of catalysts were investigated using Transmission Electron Microscopy (ThermoFisher Talos F200X). X-ray Diffraction (XRD) patterns were performed on an X-ray powder diffractometer (D/max2550 V, Rigaku Japan). High angle annular dark field (HAADF)-STEM images were recorded using a convergence semi angle of 11 mrad, and inner- and outer collection angles of 59 and 200 mrad, respectively. N_2 adsorption-desorption data were obtained at liquid nitrogen temperature (77 K) on a Micromeritics ASAP 2010 M apparatus. X-ray Photoelectron Spectroscopy (XPS) was recorded on a Thermo Scientific TM K-Alpha TM+ spectrometer with a monochromatic Al Kα X-ray source (hν =1486.6 eV) and the binding energies was referenced to the C1s peak (284.8 eV) corresponding to the adventitious carbon. The Brunauer-Emmett-Teller (BET) method was used to calculate the catalyst surface areas. Raman spectra were obtained on a Renishaw 2000 instrument with a 532 nm excitation wavelength. The metal contents of the catalysts were measured by ICP-OES (Perkin Elmer Ltd., USA).

4. Electrochemical measurements

4.0 mg of catalyst was added to a 200 μL of mixture solution in a centrifuge tube with Nafion dispersion and isopropanol in a volume ratio of 1:9. Then, catalyst was dispersed by ultrasonic for 30 min to form an even catalyst ink. 5 μL of catalyst ink was dropped onto the surface of glassy carbon rotating disk electrode (RDE, area: 0.196 cm^2) and dried naturally to form an even film with a catalyst mass loading of 0.5 mg cm^{-2}. All control samples were dropped on the electrode with the same loading. The RDE as the working electrode, the graphite rod as the counter electrode and a Hg/HgO electrode as the reference electrode. All potentials reported were calibrated to the reversible hydrogen electrode (RHE).

Oxygen was bubbled in the 0.1 M KOH solution for 30 min to form an O_2-saturated electrolyte before the ORR test. The catalysts were first active by conducting cyclic voltammetry (CV) between 0.1 and 1.1 V (*vs*. RHE) at a scan rate of 100 mV s^{-1}. Linear sweep voltammetry (LSV) was conducted to evaluate the ORR performance at a scan rate of 10 mV s^{-1} with an applied potential range from 1.1 to 0.1 V (*vs*. RHE) under the rotating speed of 1600 rpm. The CV measurement for ORR performance was conducted at a scan rate of 10 mVs^{-1}. The electrochemically active surface area (ECSA) was determined by estimating electrochemical double-layer capacitances (C_{dl}) with cyclic voltammograms in a non-faradaic region (1.00 - 1.20 V) at different scan rates (10, 15, 20, 25 and 30 mV s^{-1}). The capacitive currents, $\Delta J/2$ (ΔJ = Ja - Jc, Ja and Jc refer to anodic and cathodic current densities at 1.10 V (vs. RHE), are plotted against the scan rate and fit to a linear regression. The slope is the C_{dl}. The accelerated degradation test by cycling between 0.2 V to 1.1 V at 100 mV s^{-1} for 10000 cycles. The chronoamperometry was conducted at a potential of 0.5 V (*vs*. RHE) at room temperature with a rotating speed of 900 rpm. The electrochemical impedance spectroscopy (EIS) measurements were taken at a rotational speed of 900 rpm, encompassing a frequency spectrum from 10 kHz to 0.01 Hz, with a perturbation amplitude of 5 mV.

The electron transfer number (*n*) can be calculated according to the Koutecky-Levich (K-L) equation as follows:

$$\frac{1}{j}=\frac{1}{j_{\mathrm{l}}}+\frac{1}{j_{\mathrm{k}}}=\frac{1}{B\omega^{1/2}}+\frac{1}{j_{\mathrm{k}}} \tag{1}$$

$$B=0.2nFC_0D_0^{2/3}\upsilon^{-1/6} \tag{2}$$

in which j is the experimental disk current density, j_{l} is the diffusion-limiting current density, j_{k} is the kinetic current density, ω is the angular rotation speed of the working electrode in rad s^{-1}, F is faraday constant (96,485 C mol^{-1}), C_0 is the bulk concentration of O_2 (1.2×10^{-6} mol cm^{-3}), D_0 is the diffusion coefficient of O_2 in 0.1 M KOH solution (1.9×10^{-5} cm^2 s^{-1}), and υ is the kinetic viscosity of 0.1 M KOH solution (0.01 cm^2 s^{-1}). The K-L plots can be derived from LSV curves at different rotation speeds (400, 625, 900, 1225, 1600 rpm) under various potentials (0.30, 0.40, 0.50, 0.60, 0.70 V).

Turnover frequency (TOF, e s^{-1} $site^{-1}$) of the prepared catalysts was calculated from the below equations:

$$\mathrm{TOF}=\frac{J_k N_e M_{Fe}}{N_A W_{Fe} C_{Catal}} \tag{3}$$

where J_k represents the kinetic current density (A cm^{-2}), Ne is the electron number of per Coulomb (6.24×10^{18} C^{-1}), M_{Fe} is the molar mass of Fe (55.845 g mol^{-1}), N_A is Avogadro constant (6.022×10^{23} mol^{-1}).

For the RRDE tests, the n and hydrogen peroxide yield (% H_2O_2) were calculated by the following equations:

$$n=\frac{4\times N\times I_D}{I_R+(I_D\times N)} \tag{4}$$

$$\%H_2O_2=\frac{200\times I_R}{I_R+(I_D\times N)} \quad (5)$$

where I_D is the disk current, I_R is the ring current, and N (26%) is the collection efficiency.

5. Zinc-Air Batteries (ZABs) Performance Testing

4.0 mg of catalyst was added to a 200 μL of mixture solution in a centrifuge tube with Nafion dispersion and isopropanol in a volume ratio of 1:9. Then, catalyst was dispersed by ultrasonic for 30 min to form an even catalyst ink. 5 μL of catalyst ink was dropped onto the carbon fiber paper, achieving a final area of 1.0 cm2. Finally, the carbon fiber paper, gas diffusion layer, and nickel foam were conducted as the cathode and the zinc plate was conducted as the anode, and mixed solution of Zn $(Ac)_2$ (0.2 M) and KOH (6.0 M) as the electrolyte.

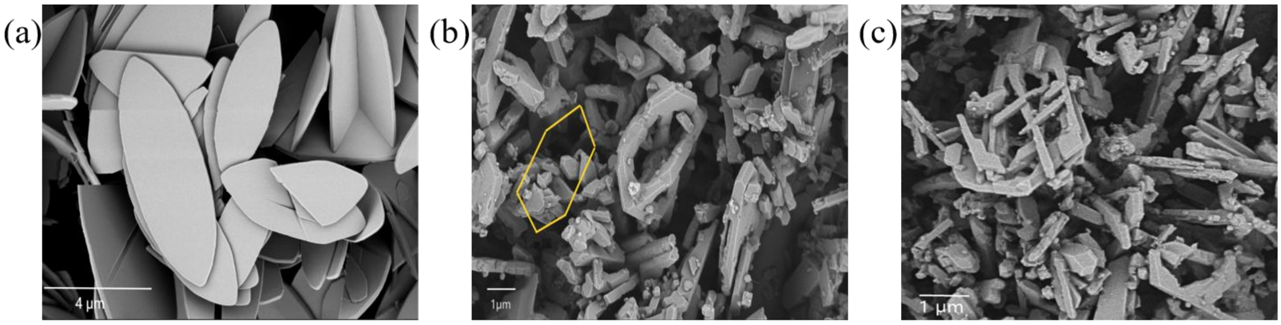

Figure S1: SEM images of (a) ZIF-L, (b) pNC and (c) ZIF-R.

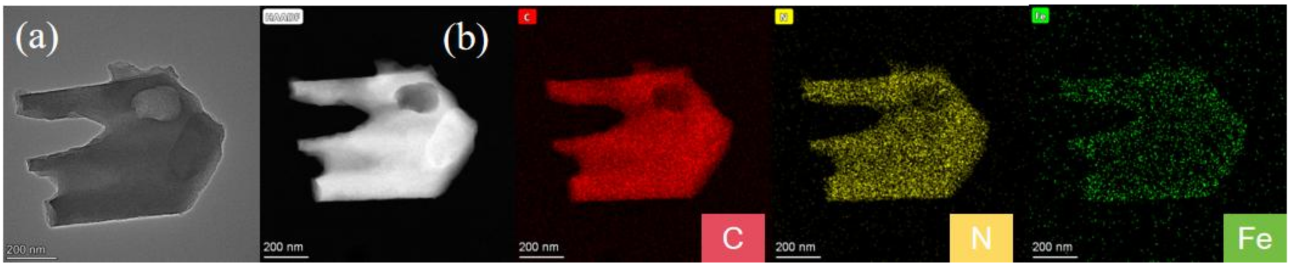

Figure S2: (a) HR-TEM, (b) HAADF-STEM, and corresponding elemental mapping of Fe-N-C

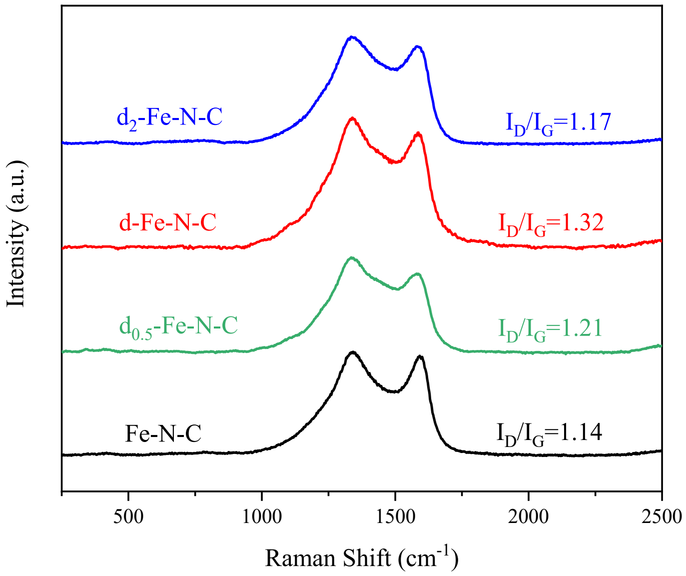

Figure S3: Raman patterns of d$_x$-Fe-N-C (x = 0.5, 1, 2) and Fe-N-C.

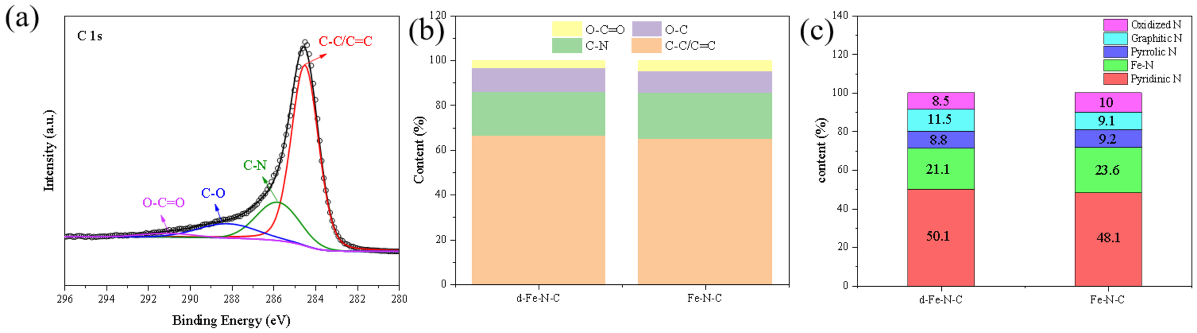

Figure S4: (a) High-resolution C 1s XPS spectra of d-Fe-N-C. (b) Contents of different C species and (c) N species in the d-Fe-N-C and Fe-N-C.

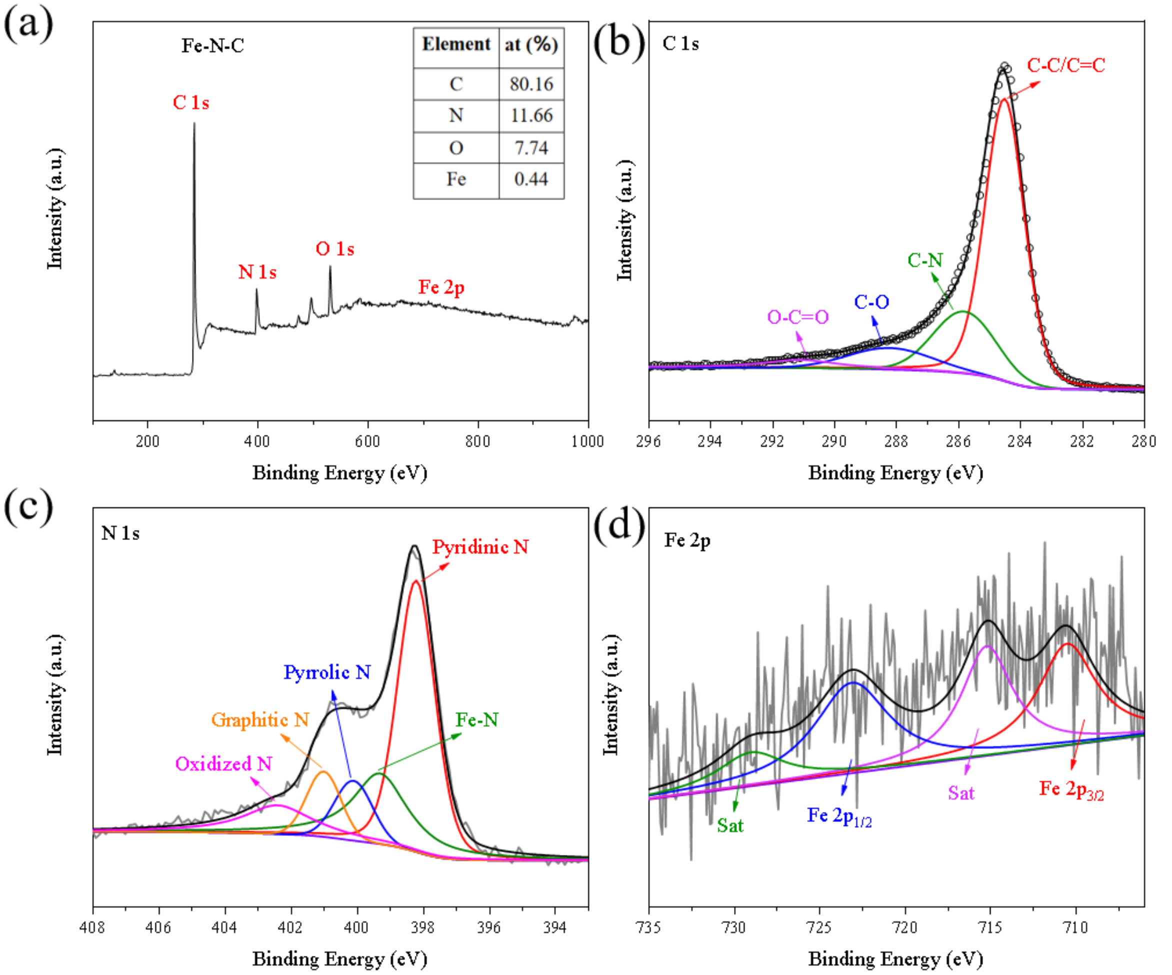

Element	at (%)
C	80.16
N	11.66
O	7.74
Fe	0.44

Figure S5: (a) XPS survey spectra of electrocatalysts. (b) High-resolution C 1s, (c) N 1s and (d) Fe 2p XPS spectra of Fe-N-C.

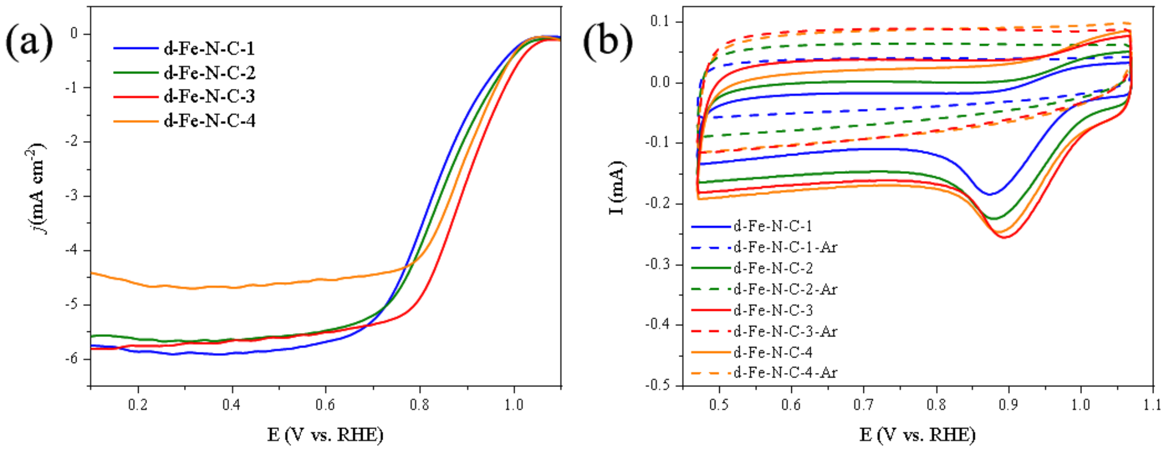

Figure S6: (a) LSV curves at 1600 rpm and (b) CVs of d-Fe-N-C-x (x=1, 2, 3, or 4 mg) in O_2-saturated 0.1 M KOH solution.

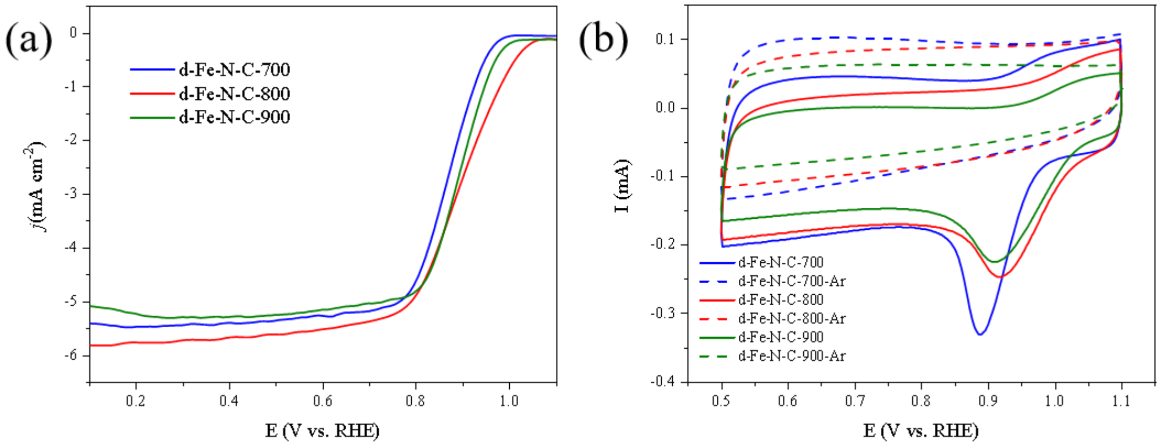

Figure S7: (a) LSV curves at 1600 rpm and (b) CVs of d-Fe-N-C-T (T = 700, 800, 900°C) in O_2-saturated 0.1 M KOH solution.

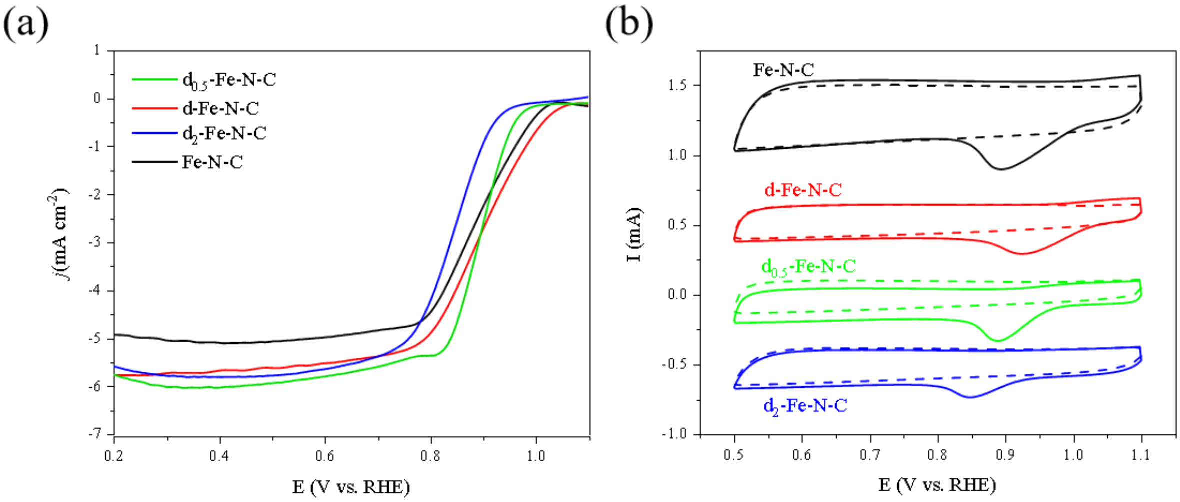

Figure S8: (a) LSV curves at 1600 rpm and (b) CVs of d_x-Fe-N-C (x = 0.5, 1, 2) and Fe-N-C in O_2-saturated 0.1 M KOH solution.

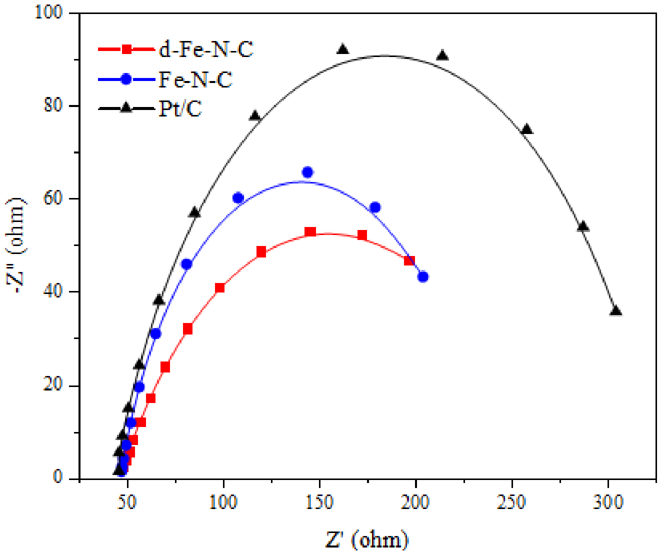

Figure S9: EIS curves of the d-Fe-N-C, Fe-N-C and Pt/C.

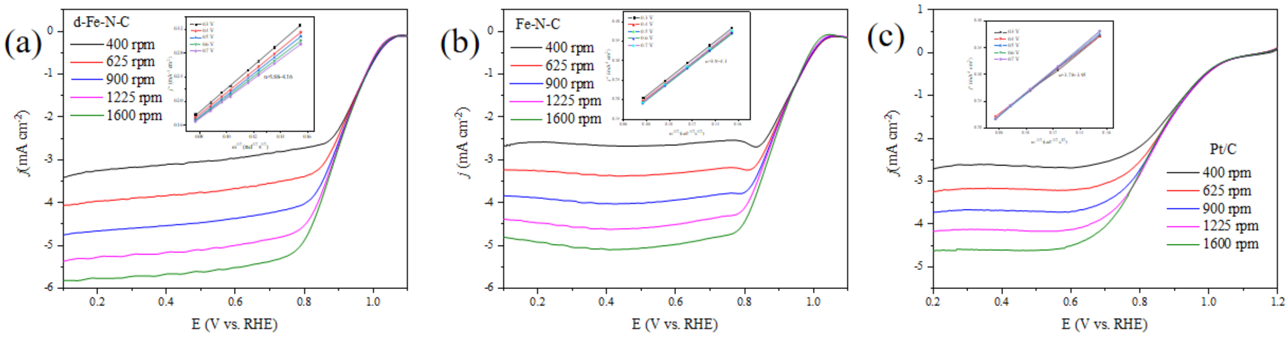

Figure S10: ORR polarization curves at different rotating speeds and fitted K-L plots at 0.3-0.7V of (a) d-Fe-N-C, (b) Fe-N-C, and (c) Pt/C in O_2-saturated 0.1 M KOH.

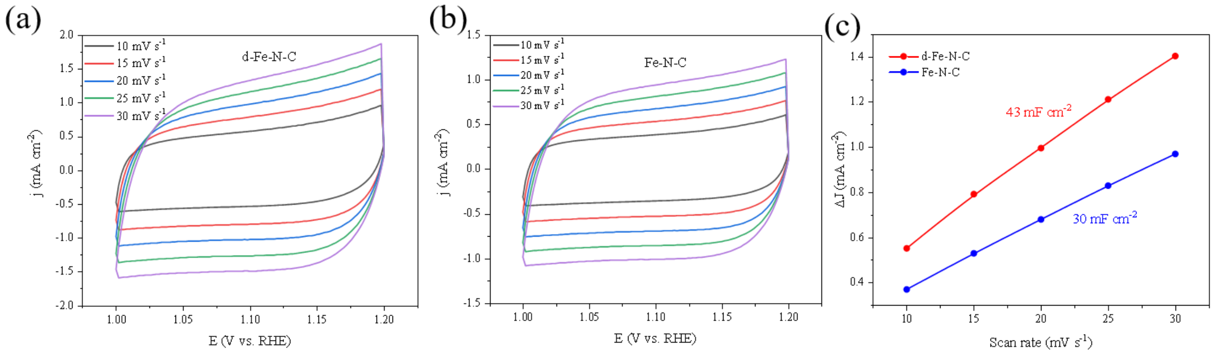

Figure S11: CV curves at 1.0-1.2 V (vs. RHE) with various scan rates of (a) d-Fe-N-C, (b) Fe-N-C, and (c) the corresponding Cdl of d-Fe-N-C and Fe-N-C.

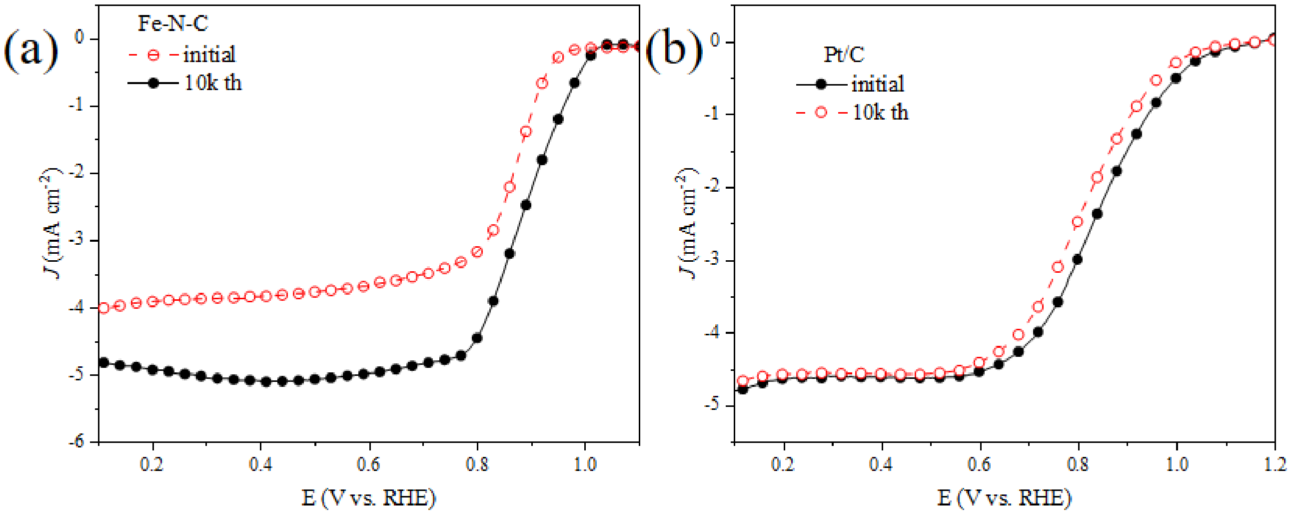

Figure S12: LSV curves of (a) Fe-N-C and (b) Pt/C before and after the 10,000 cycles of potential scanning from 0.2 V to 1.1 V at 100 mV s-1 in O2-saturated 0.1 M KOH solution.

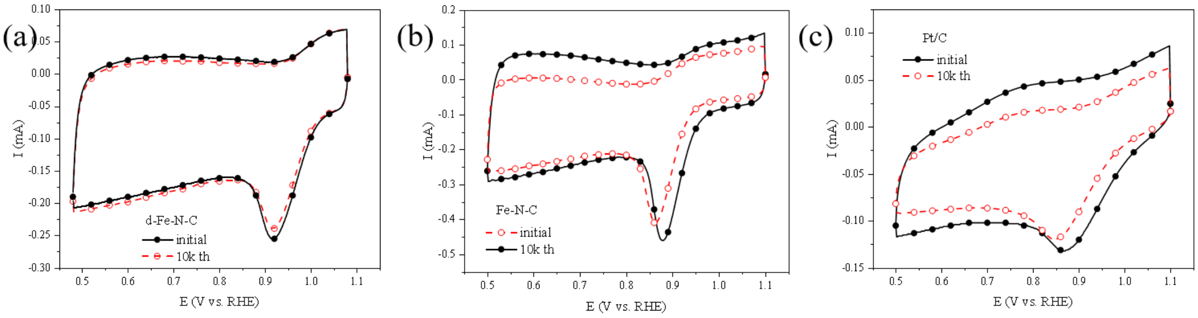

Figure S13: CV curves of (a) d-Fe-N-C, (b) Fe-N-C, and (c) Pt/C before and after the 10,000 cycles ADT.

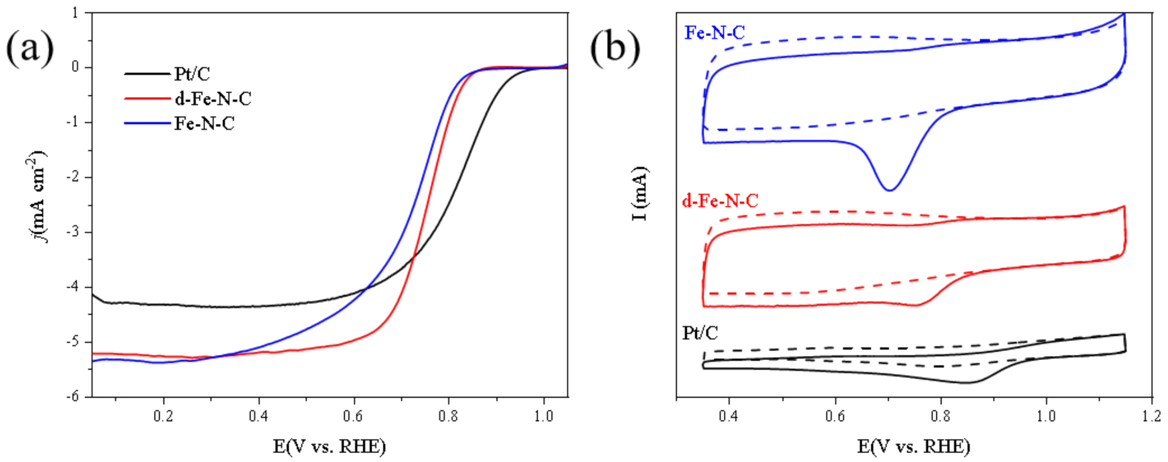

Figure S14: (a) LSV curves and (b) CV of different catalysts in O_2-staurated 0.1 M $HClO_4$ solution at 1600 rpm.

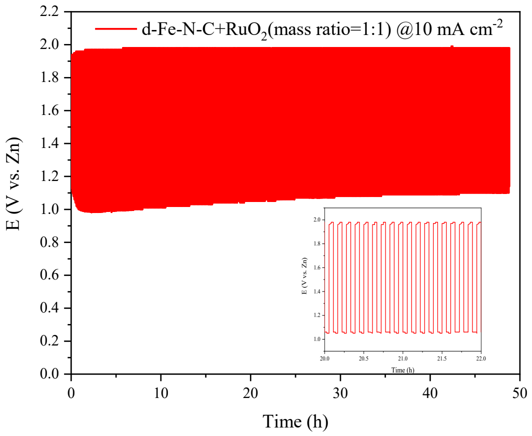

Figure S15: Charge-discharge curve of d-Fe-N-C-loaded ZABs at 10 mA cm^{-2}.

Table S1. The content of different element for the prepared catalysts calculated from XPS.

Sample	Fe (at%)	N (at%)	C (at%)	O (at%)
d-Fe-N-C	0.46	11.95	80.08	7.51
Fe-N-C	0.44	11.66	80.16	7.74

Table S2. The content of metal element for the prepared catalysts calculated from ICP-OES.

Sample	Fe (wt%)
d-Fe-N-C	1.57
Fe-N-C	1.52

Table S3. The content of different C species for the prepared catalysts calculated from XPS.

Sample	C-C/C=C	C-N	C=O	O=C-O
d-Fe-N-C	66.7 %	19.4 %	10.5 %	3.4 %
Fe-N-C	65.1 %	20.5 %	9.7 %	4.7 %

Table S4. The content of different N species for the prepared catalysts calculated from XPS.

Sample	Pyridinic N	Fe–N	Pyrrolic N	Graphitic N	Oxidized N
d-Fe-N-C	50.1 %	21.1 %	8.8 %	11.5 %	8.5 %
Fe-N-C	48.1 %	23.6 %	9.2 %	9.1 %	10 %

Table S5. Comparison of the Fe content determined by ICP-OES in the d-Fe-N-C catalyst before and after long-term testing.

	Fe (wt%)
Before	1.57
After	1.56

Table S6. Comparison of ORR performance of previously reported iron-based catalysts.

Catalysts	**Electrolyte**	**$E_{1/2}$ (V vs. RHE)**	**Reference**
d-Fe-N-C	0.1 M KOH	0.91	This work
Fe-Nv-C SAC	0.1 M KOH	0.902	[2]
e1-Fe-N-C	0.1 M KOH	0.876	[3]
Fe–N–C-E	0.1 M KOH	0.92	[4]
Fe-SA/HPC	0.1 M KOH	0.91	[5]
Fe-N-DCSs	0.1 M KOH	0.90	[6]
Defects-FeNC	0.1 M KOH	0.895	[7]
G-Fe-N-C	0.1 M KOH	0.861	[8]
F–Fe–N–C	0.1 M KOH	0.91	[9]
Fe–N–C SACs	0.1 M KOH	0.910	[10]
r-Fe–NC	0.1 M KOH	0.90	[11]
Fe SA@NCZ	0.1 M KOH	0.92	[12]
FePc/SWCNT	0.1 M KOH	0.952	[13]
Fe_{nc}/Fe_1-N-C	0.1 M KOH	0.931	[14]
Fe-N/O(5.2)/OMC	0.1 M KOH	0.94	[15]

References

[1] Lee S, Oh S, Oh M. A typical Hybrid Metal–Organic Frameworks (MOFs): A Combinative Process for MOF-on-MOF Growth, Etching, and Structure Transformation. *Angew. Chem. Int. Ed.*, 2020, *132*, 1343-1349.

[2] Jia B, Xie X, Lin J, et al. Harnessing Pyridinic N Vacancy Defect in Microporous Structures to Induce the Pre-Adsorption of Oxygen and Boost Oxygen Reduction Reaction Kinetics. *Angew. Chem. Int. Ed.*, 2025, *64*, e202508674.

[3] Pang R, Xia H, Dong X, et al. Zinc Assisted Thermal Etching for Rich Edge-Located Fe-N_4 Active Sites in Defective Carbon Nanofiber for Activity Enhancement of Oxygen Electroreduction. *Adv. Sci.*, 2024, *11,* 2407294.

[4] Li X, Ye G, Zhu W, et al. Directional construction of low-coordination Fe–N3 coupled with intrinsic carbon defects for high-efficiency oxygen reduction. *ACS Nano*, 2024, 18, 24505-24514.

[5] Wu S, Liu H, Lei G, et al. Single-atomic iron-nitrogen 2D MOF-originated hierarchically porous carbon catalysts for enhanced oxygen reduction reaction. *Chem. Eng. J.*, 2022, *441*, 135849.

[6] Liu Y, Zong L, Zhang Y, et al. Joule heating synthesis for single-atomic Fe sites on porous carbon spheres and armchair-type edge defect engineering dominated oxygen reduction reaction performance. *Appl. Catal. B: Environ. Energy*, 2025, *361*, 124673.

[7] Yang K Z, Xu C, Guo P P, et al. Creating Defects in the Active Site of Fe-N-C Catalyst Promotes Catalytic Performance for Oxygen Reduction Reaction. *ChemNanoMat*, 2023, *9*, e202300138.

[8] Zhang L, Su H, Yang F, et al. Molten-salt-assisted guanine-derived Fe-N-C electrocatalyst for oxygen reduction reaction. *J. Environ. Chem. Eng.*, 2025, *13*, 115067.

[9] Wang X, Li K, Zeng Y, et al. Dynamic Fe— F Coordination Triggered Structure-Adaptive Fe–N–C for Efficient Oxygen Reduction Electrocatalysis. *Angew. Chem. Int. Ed.*, 2025, 137, e202513102.

[10] Liang R, Wang J, Zhai Y, et al. Synthesis of Fe-N-C Single-Atom Catalysts with a Facile Salt-Templated Strategy for Efficient and Stable Oxygen Reduction Reaction. *ACS Appl. Energy Mater.*, 2025, *8*, 15911-15921.

[11] Wang Q, Lu R, Yang Y, et al. Tailoring the microenvironment in Fe-N-C electrocatalysts for optimal oxygen reduction reaction performance. *Sci. Bull.*, 2022, *67*, 1264-1273.

[12] Tan S, Wang R, Dong J, et al. Molecular Self-assembly Directed Edge Engineering of Lignin-Derived Fe-N-C Single-Atom Catalysts for Efficient Oxygen Reduction Reaction. *Energy Storage Mater.*, 2025, 104729.

[13] Charles B. Musgrave III, Su J, Xiong P, et al. Molecular strain accelerates electron transfer for enhanced oxygen reduction. *J. Am. Chem. Soc.*, 2025, 147, 3786-3795.

[14] Yu J, Fan H S, Liang X, et al. Fe Clusters Liganded Single-Atom Fe-N-C Hollow Nanosheets as Bifunctional Catalysts for Stable Zn— air/Iodide Hybrid Batteries. *Adv. Sustain. Syst.*, 2025, 9, e01217.

[15] Pei C, Yao G, Zhao Z, et al. eg Electron Occupancy as a Descriptor for Designing Iron Single-Atom Electrocatalysts. *Adv. Mater.*, 2025, 37, 2504852.